A robotic system for crystallizing membrane and soluble proteins in lipidic mesophases

Vadim Cherezov, Avinash Peddi, Lalitha Muthusubramaniam, Yuan F. Zheng and Martin Caffrey

A robotic system for crystallizing membrane and soluble proteins in lipidic mesophases

**Vadim Cherezov,[a] Avinash
Peddi,[b] Lalitha
Muthusubramaniam,[c] Yuan F.
Zheng[b] and Martin Caffrey[d,e]***

[a]Department of Chemistry, The Ohio State
University, Columbus, OH 43210, USA,
[b]Department of Electrical and Computer
Engineering, The Ohio State University, OH
43210, USA, [c]Department of Biomedical
Engineering, The Ohio State University,
Columbus, OH 43210, USA, [d]Departments of
Chemistry, Biophysics and Biochemistry, The
Ohio State University, Columbus OH 43210,
USA, and [e]University of Limerick, Limerick,
Ireland

Correspondence e-mail: martin.caffrey@ul.ie

A high-throughput robotic system has been developed for crystallizing membrane proteins using lipidic mesophases. It incorporates commercially available components and is relatively inexpensive. The crystallization robot uses standard automated liquid-handlers and a specially built device for accurately and reproducibly delivering nanolitre volumes of highly viscous protein/lipid mesophases. Under standard conditions, the robot uses just 20 nl protein solution, 30 nl lipid and 1 µl precipitant solution. 96 wells can be set up using the robot in 13 min. Trials are performed in specially designed 96-well glass plates. The slim (<2 mm high) plates have exquisite optical properties and are well suited for the detection of microcrystals and for birefringence-free imaging between crossed polarizers. Quantitative evaluation of the crystallization progress is performed using an automated imaging system. The optics, in combination with the slim crystallization plates, enables in-focus imaging of the entire well volume in a single shot such that a 96-well plate can be imaged in just 4.5 min. The performance characteristics of the robotic system and the versatility of the crystallization robot in performing vapor-diffusion, microbatch and bicelle crystallizations of membrane and soluble proteins are described.

1. Introduction

Crystallography is the most reliable way to explore membrane-protein structure–function relationships in atomic detail. To perform crystallography requires crystals, which are not readily procured in the case of membrane proteins. Part of the problem is the dearth of usable quantities of pure and active membrane proteins. The other problem concerns the production of diffraction-quality crystals.

To date, over 50 different membrane-protein structures have been deposited in the Protein Data Bank (http://www.rcsb.org). The bulk of these have been determined using crystals that have been grown using well established vapor-diffusion techniques in combination with an assortment of solubilizing surfactants (herein referred to as the *in surfo* method). Over the past several years, newer methods have emerged that exploit the ability of lipids to form liquid crystals or mesophases and to reconstitute membrane proteins (reviewed in Caffrey, 2003). These are collectively referred to as *in meso* methods. One of these is based on the lipidic cubic phase (Nollert *et al.*, 2001), while another makes use of lipid/detergent bicelles (Faham & Bowie, 2002). The former has produced crystal structures of a number of important membrane proteins and helped to elucidate the photocycle in the light-driven proton pump bacteriorhodopsin in atomic detail. Indeed, the highest resolution structure of any membrane protein (bacteriorhodopsin at 1.43 Å; Schobert *et*

DOI: 10.1107/S0907444904019109 **1795**

al., 2002; Lanyi & Schobert, 2002) was obtained using this modification of the *in meso* method. However, the yield of the method has not been impressive. The sense is that this in part relates to perceived difficulty in performing *in meso* crystallization and reluctance on the part of the community to use the method. Much of the hesitancy originates from the fact that the method involves manipulating extremely viscous lipidic dispersions.

In the recent past, we have introduced a mixing device that facilitates the handling of small quantities of such viscous lipidic materials (Cheng *et al.*, 1998). This has been adapted to *in meso* crystallization. Furthermore, we have developed inexpensive glass-based crystallization plates and a dispensing device that enables *in meso* crystallization trials of membrane proteins to be set up with ease (Cherezov & Caffrey, 2003). However, the latter advances are limited by virtue of the fact that the entire process must be performed by hand. Thus, manual dexterity, patience and good visual acuity are required of the user, especially when nanolitre volumes of materials are being dispensed. For many membrane proteins, crystallizations must be set up under 'hostile' conditions such as at frigid temperatures and in the dark or under reduced light.

Figure 1
The 96-well glass sandwich plate used for crystallization with the *in meso* robot. (*a*) Schematic diagram of the plate. Dimensions are given in millimetres. A bar-code label is shown at the left end of the plate. (*b*) A fully loaded and sealed 96-well crystallization plate. Each well contains 50 nl cubic phase and 1 µl precipitant solution. For clarity, the cubic phase has been stained with Sudan Red and the precipitant solution includes Methylene Blue. The row and column labeling referred to in the text is indicated.

Throughput is therefore severely limited by the current instrumentation.

Crystallization trials are characterized by the need to process large numbers of samples as the multidimensional crystallization space is explored for crystal nucleation and growth. With the *in meso* methods there is the additional need to include lipid identity and concentration as a variable to be explored. This only adds to the number of trials that must be performed. There is also pressure to miniaturize and to scale down when membrane proteins and lipids are involved since they come at a premium.

We have responded to these assorted challenges (the need for automation, high throughput and miniaturization) by building a robot for *in meso* crystallization of membrane proteins. The robot was designed to meet the above specifications and for a limited budget. It consists for the most part of commercially available components that have been assembled in a way that realises these objectives. The robot is robust and performs reliably. Here, we report on our experience with the equipment over a three-month period. Home-made glass-based 96-well plates have been built for use with the robot. They offer unparalleled optical performance and allow the detection of microcrystals and birefringence-free viewing. With a profile height of <2 mm, high-density plate storage is possible. Under standard conditions, *in meso* crystallization trials are performed with 50 nl protein/lipid mesosphase [representing 20 nl protein solution (200 ng protein at 10 mg protein per millilitre)] and 1 µl precipitant solution per trial. A single 96-well plate can be set up in 13 min. The robot is quite versatile and has been adapted to perform vapor-diffusion, microbatch and bicelle crystallizations of membrane and soluble proteins.

In addition to the crystallization robot, we have built an imaging system for automatic recording and processing of well-content images. It has an optical system with a depth of field that matches the sample thickness so that only a single image must be recorded to view the entire well contents. Image acquisition from a 96-well plate takes less than 5 min. Both the crystallization and the imaging robot are described in this communication.

2. Materials and methods

2.1. Materials

Salts for buffers and precipitant solutions were of the highest quality available and were purchased from Sigma–Aldrich (St Louis, MO, USA). *n*-Octyl-*β*-D-glucoside (OG, Anagrade, Lot OG17) and 3-[(3-cholamidopropyl)-dimethyl-ammonio]-2-hydroxy-1-propane sulfonate (CHAPSO, Anagrade, Lot CHO08) were obtained from Anatrace Inc. (Maumee, OH, USA). Monoolein (1-oleoyl-*rac*-glycerol, Lot M239-MA26-N) came from Nu Chek Prep Inc. (Elysian, MN, USA) and 1,2-dimyristoyl-*sn*-glycero-3-phosphocholine (DMPC, Lot 140PC-160) was from Avanti Polar Lipids Inc. (Alabaster, AL, USA). Detergents and lipids were used as supplied. Chicken egg-white lysozyme (Lot 072K7062) was
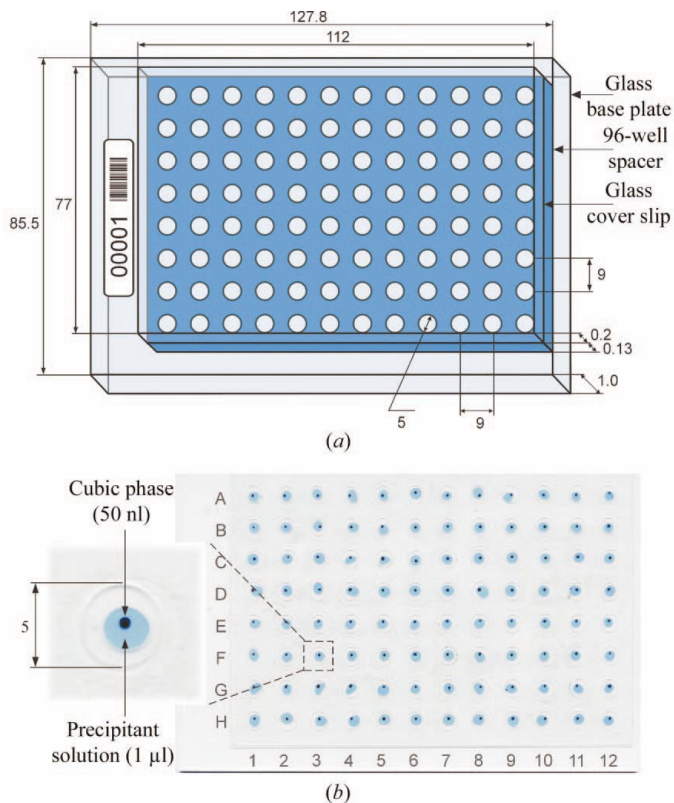
purchased from Sigma–Aldrich and used fresh without further purification. Bacteriorhodopsin (bR) was solubilized with OG from purple membrane isolated from *Halobacterium salinarum* (strain S9) using established protocols (Dencher & Heyn, 1982). Protein crystallization screen kits were obtained from Hampton Research (Aliso Viejo, CA, USA; Crystal Screen HT, Index HT, SaltRx HT), deCODE Biostructures Group (Bainbridge Island, WA, USA; Wizard I and II) and Jena Bioscience (Jena, Germany; JBScreen). Water (resistivity > 18 $M\Omega$ cm^{-1}) was purified using a Milli-Q Water System (Millipore Corporation, Bedford, MA, USA) consisting of a carbon-filter cartridge, two ion-exchange filter cartridges, an organic removal cartridge and a terminal 0.22 µm filter.
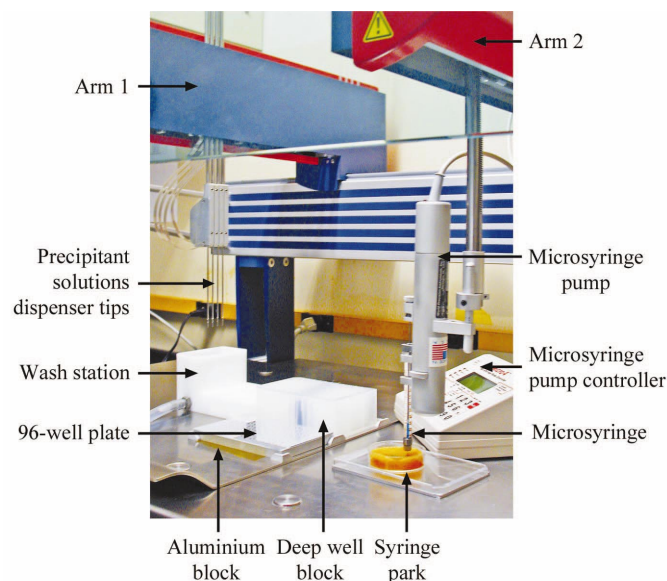
2.2. Crystallization plates

The plates used in the current application were designed specifically for use with the *in meso* robot. They are modeled on a similar but smaller plate developed for manual *in meso* crytallization (Cherezov & Caffrey, 2003). The plate has three components: a flat glass base plate, a perforated 96-hole polymeric spacer and a glass cover slip (Fig. 1*a*). The base plate (Erie Scientific, Portsmouth, NH, USA) has a footprint of 127.8×85.5 mm and conforms to the Society for Biological Screening (SBS) standard for microplates. The plate is 1 mm thick. The spacer is made from 3M double-stick (acrylic glue) polyester film that is 0.13 mm thick (Saunders East, Lombard, IL, USA). The film is cut into sections of 112×77 mm and contains 96 holes, each 5 mm in diameter with a standard 9 mm separation (Fig. 1*a*). The spacer sits atop the base plate and when filling is complete the glass cover slip (0.2 mm thick, Erie Scientific, Portsmouth, NH, USA) is placed over and onto the spacer, creating 96 individually sealed and isolated wells. The cubic phase bolus is sandwiched between and in intimate contact with the upper and lower glass plates. This arrangement gives the best possible optical properties with which to view well contents for crystal growth. An example of a loaded and sealed plate set up for *in meso* crystallization is shown in Fig. 1(*b*).
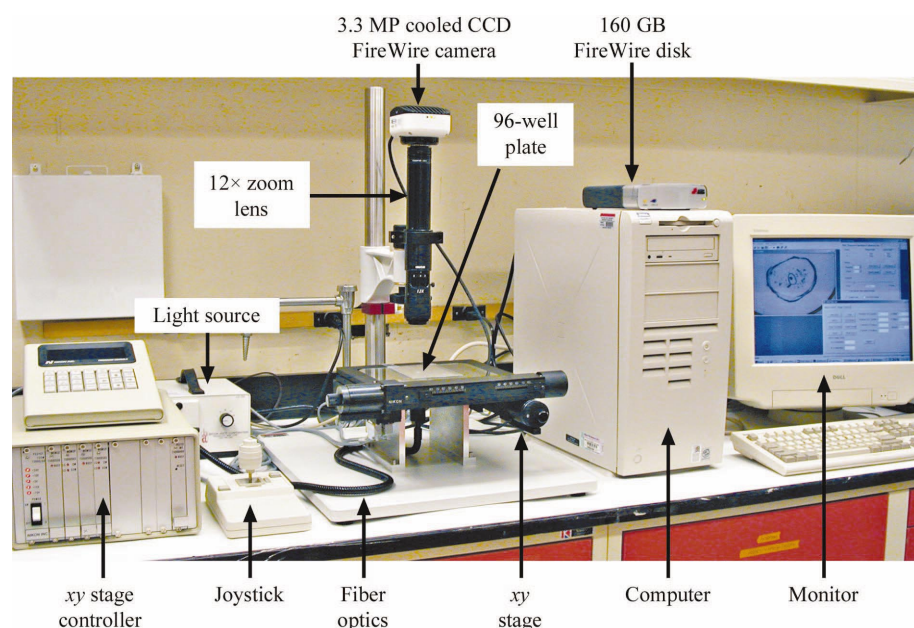
2.3. Crystallization robot

The robot was designed and built first and foremost to perform automated crystallization of membrane proteins using the *in meso* method. However, as will be demonstrated below, it also works with other crystallization protocols. The robot was built based on Xantus, a commercially available liquid-handling robot (Sias US, New Castle, DE, USA; Fig. 2). The open style, modular design and software flexibility of the Xantus allowed us to adapt it so that it would perform the steps needed for *in meso* crystallization. The standard Xantus robot consists of a 1×0.7 m deck with two independent arms. Arm 1 is used for liquid aspiration and dispensing, while arm 2 is typically a plate gripper and moving device. We retained the original function of arm 1

Figure 2
The *in meso* crystallization robot. The major parts of the robot referred to in the text are labeled. The robot has two dispensing arms. Arm 1 includes four tips and is used for handling liquid precipitant solutions. Arm 2 supports a microsyringe for dispensing the protein/lipid dispersion (mesophase). The microsyringe dispenses mesophase by the action of a microsyringe pump which in turn is driven by a controller. When not in use, arm 2 goes to a park position where the microsyringe needle tip is placed in a moist sponge. The cubic phase in the syringe is stained with Methylene Blue for clarity. Also shown in the figure are a 96-well glass plate, a 96-deep-well block of precipitant solutions and a station where the tips on arm 1 are washed.

Figure 3
The imaging robot for automatic screening of 96-well glass sandwich crystallization plates.

and equipped it with four small-volume liquid-handling tips for pick-up and placement of precipitant solutions. Arm 2 was modified to handle the viscous protein/lipid mesophase. To this end, the gripper device was replaced with a motor-driven positive-displacement Hamilton syringe (UMP II with Micro4 controller, World Precision Instruments, Sarasota, FL, USA). The controller for the latter was interfaced to the Xantus through an RS-232 cable. The positional accuracy of arm 2 was raised by increasing the gear ratio of the z motor by a factor of 8.

2.4. Imaging station

The imaging station was designed in-house. It was assembled and delivered by Brook-Anco Corporation, Rochester, NY, USA. The station includes the following components (Fig. 3): a $12\times$ zoom lens (Navitar, Rochester, NY, USA), a 3.3 MP MicroPublisher RTV 3.3 cooled CCD camera (Qimaging, Burnaby, BC, Canada), a BioPrecision xy table with MAC 2000 controller (Ludl Electronic Products Ltd, Hawthorne, NY, USA), fiber optics with IR-cutoff and neutral light filters (Schott North America Inc., Southbridge, MA, USA), a spot lens (Schott North America Inc.) and a linear polarizer and a rotating analyzer (Midwest Optical Systems, Palatine, IL, USA). The choice of optics and CCD camera was made with a view to enabling the entire sample (130 µm thick) to be within the depth of field of the imaging device with the best possible resolution. The xy translation table has a travel of 160 mm in both x and y directions, with a resolution (step size) of 0.2 µm, a repeatability of 1 µm and an accuracy of 6 µm. Transmitted illumination from a halogen DDL lamp is provided through a fiber optic with an attached IR-cutoff filter, a neutral light filter and a linear polarizer. The light from the fiber optic is focused on the sample using the spot lens. The camera is connected to a computer through the FireWire port and the xy-table controller is connected to the computer through the RS-232 port. A computer program that controls the plate-scanning process was written in C++. It allows plate alignment, setup of camera parameters, automatic scanning of all 96 wells and storage of raw images on an external 160 GB FireWire disk. Imaging and data storage for a 96-well plate takes ~4.5 min. Raw images are subsequently batch-processed to perform Bayer interpolation, white balance and image enhancement. Processed images are stored as JPEG files identified by plate and well number and scan date. Processed images are inspected and scored by skilled personnel using a computer screen (22 inch, 1600×1200 pixels).

2.5. Crystallization trials

2.5.1. In meso crystallization. *In meso* crystallization begins with an initial mixing of the protein solution with the lipid. In this step, the mesophase forms spontaneously and in the case of membrane proteins the protein is assumed to reconstitute into the lipid bilayer. Homogenization is carried out in a syringe mixer (Cheng *et al.*, 1998) using 60%(w/w) monoolein and 40%(w/w) protein solution [15 mg ml^{-1} bR in 25 mM sodium potassium phosphate buffer pH 5.6 (SPP) or

50 mg ml^{-1} lysozyme in 0.1 M sodium acetate buffer pH 4.8, as described by Misquitta & Caffrey (2003)]. The protein-laden mesophase is then transferred to a 100 µl gas-tight syringe (Hamilton Company, Reno, NV, USA) fitted with a 10 mm long removable needle (gauge 26, 'blunt needle-point style'). The syringe is mounted on arm 2 of the robot and its plunger is engaged with the motorized pump mechanism. A 96-deep-well block of precipitant solutions and the 96-well glass plate/spacer combination are put into position on the deck of the robot. The x, y, z coordinates of the center of the first well in the plate are found by adjusting the position of arm 2 until the tip of the syringe needle just touches the base plate. This last step takes about 5 min to complete. The same z-setting is reliable for a set of at least 12 plates. The coordinates are entered into the robot controller and robotized dispensing of mesophase and precipitants commences. This takes place in the following order. The first four wells are loaded sequentially with 50 nl of cubic phase. Arm 2 moves to the park position away from the plate and stabs the syringe needle into a moist sponge. This serves a double duty: to prevent dehydration of the cubic phase in the tip of the needle during storage and to clean the tip of any carry-over mesophase. While parked, arm 1 with its four tips is activated to simultaneously aspirate four different precipitant solutions from the precipitant block and to dispense 1 µl of each over the cubic phase boluses sitting in the first four wells. Arm 1 moves to the wash station where the residual precipitants in the tips are expelled and the inside and outside of the tips are washed and rinsed with Milli-Q water. Arm 1 then moves to its own park position. This description represents a full cycle, which is repeated 24 times until all 96 wells are filled. The wells are capped with the glass cover slip and a soft rubber brayer is used to effect tight sealing. The sealed plate is placed in a temperature-controlled incubator at 293 K for crystallization to occur. The entire process of loading and sealing a single 96-well plate takes about 13 min to complete. The total time to mix lipid and protein and to fill 12 plates is ~4 h.

2.5.2. Microbatch cystallization. Microbatch crystallization can be performed using the *in meso* robot in a way that is almost identical to the standard *in meso* protocol. The only difference is that a solution, as opposed to a viscous lipidic dispersion, is used in the microsyringe of arm 2 of the robot as the source of protein. Typically, microbatch is performed with equal volumes of protein and precipitant solutions. Since the smallest volume of precipitant deliverable using arm 1 of the robot is 0.5 µl, the volume of protein solution dispensed by the microsyringe on arm 2 was increased to this value. To minimize shock nucleation, the protein solution is dispensed first, followed by the precipitant solution. No mechanical mixing of the two solutions is performed. Upon filling all 96 wells, the plate is capped and sealed with a glass cover slip, as above.

While 96-well glass sandwich plates were used in this application, microbatch crystallization can equally well be carried out in commercially available SBS standard 96-well plates.

2.5.3. Sitting-drop crystallization. The *in meso* robot can also be used to perform vapor-diffusion sitting-drop crystal-

lization trials. For this purpose, 96-well Corning CrystalEX sitting-drop microplates (Hampton Research, Aliso Viejo, CA, USA) were used. Precipitant and protein solutions were dispensed by arms 1 and 2 of the robot, respectively. The procedure begins with the delivery of 0.5 µl protein solution into the first four protein wells. Arm 1 is subsequently activated to pick up and dispense four precipitant solutions simultaneously: 50 µl to the reservoirs, followed by 0.5 µl to the protein wells. The cycle is repeated 24 times to complete the 96-well plate, which is then sealed with transparent three-inch-wide crystal clear sealing tape (Hampton Research, Aliso Viejo, CA, USA). The entire process takes about 13 min to complete.

2.5.4. Bicelle crystallization. Bicelle preparation and bR reconstitution into bicelles were performed as previously described (Faham & Bowie, 2002). Briefly, a dispersion consisting of 33%(w/w) DMPC in water was prepared and added to powdered CHAPSO at a DMPC:CHAPSO molar ratio of 3. It was homogenized by temperature cycling between 253 and 313 K coupled with vortex mixing at 277 K. When thoroughly mixed, a transparent optically clear bicelle solution was obtained in the range ∼273–293 K. Above 298 K, a transparent optically clear viscous gel forms. bR was reconstituted into the bicelles directly from purple membrane (PM). To this end, four volumes of PM dispersion (∼10 mg ml^{-1} bR in water) were combined with one volume of bicelle solution followed by gentle mixing at 277 K. This produced a bicellarized bR solution containing ∼8 mg ml^{-1} bR and 8%(w/w) DMPC/CHAPSO (3:1 molar ratio) bicelles which can be used directly in crystallization trials.

The original bicelle crystallization method was developed using the vapor-diffusion hanging-drop technique (Faham & Bowie, 2002). We observed, however, that the bicelle crystallization of bR could also be performed by the microbatch method using the *in meso* robot and the glass sandwich plates described above. Accordingly, the microsyringe pump on arm 2 was used to deliver 400 nl bicelle/protein solution and the pipettes on arm 1 dispensed 0.5 µl precipitant into each well. The precipitants used in this study consisted of sodium dihydrogen phosphate in the concentration range 3–5 M. Eight concentrations were used to create 12 replicates of each on the 96-well plate. Thus, rows A–H had different concentrations of precipitant, with the highest in row A progressing to the lowest in row H (see plate layout in Fig. 1). Replicates were arrayed in columns numbered 1–12. Wells were filled in the following order: A1, B1, ..., A2, B2, ..., G12 and H12. Since evaporation occurs during the course of setting up the trials, the degree of evaporation and thus the final concentration of protein and other ingredients in the well vary across the plate. This is advantageous to the screening process since a greater number of conditions can be evaluated. The bicelle crystallization trials reported on in this study were performed in a room at ∼30% RH and without local humidification. Under these conditions we expected that the maximum degree of water loss across the plate would amount to greater than 30% (see below).

2.6. Screening

The contents of each well in a plate must be examined individually to evaluate the crystallization trial. Currently this is performed in the laboratory using a combination of manual screening and automatic imaging coupled with manual evaluation. The screening schedule adhered to after trials are set up is as follows: day 1, manual; day 3, automatic; day 7, manual; day 14, automatic; day 28, manual. Manual screening requires that the researcher examines the plates on a Nikon E-400 microscope equipped with 4×, 10× and 40× objectives, a polarizer and a rotating analyzer. Automated screening makes use of the imaging station introduced above. Images are recorded in normal light and between crossed polarizers and are inspected and scored by qualified personnel. Observations are recorded into spreadsheets using a 0–9 crystallization rating scale developed specially for *in meso* work. Voice confirmation of numerical scoring and data entry has been implemented. This facilitates the annotation process since the person screening does not have to look away from the microscope and at the computer screen to verify that the correct score has been entered. This was performed using a program called *Narrator* that comes with Microsoft Windows XP.

2.7. Robot performance characterization

Accuracy and precision of the *in meso* robot as far as delivery volume is concerned were evaluated by direct imaging. Thus, desired volumes of precipitant or lipidic mesophase were dispensed in replicate into wells of a 96-well glass crystallization plate. The plate was sealed with a glass cover slip in such a way that the precipitant solution or the mesophase was sandwiched between the two glass plates. The plate was scanned immediately using the imaging robot with 1× and 3× magnification, respectively, in the case of precipitant solutions and the lipidic mesophase. The images were analyzed using *Adobe Photoshop* (Adobe Systems, Inc., San Jose, CA, USA) or *ImageJ* (Wayne Rasband, NIH, Bethesda, MD, USA; available free from http://rsb.info.nih.gov/ij/) programs to determine the area occupied by the precipitant drop or the bolus of mesophase. Volumes were calculated as the product of the area and the well spacer thickness (130 µm). The cubic phase boluses used for quantitative analysis were not covered with precipitant solutions and had a uniform disc shape after being compressed between the two glass plates. In addition, the average dispensing volume was calibrated by checking the actual movement of the syringe plunger after 100 deliveries of a fixed volume.

3. Results and discussion

3.1. Crystallization plates

These plates were designed for *in meso* crystallization of membrane proteins. As noted, they have been adapted for other types of crystallizations. With regard to the *in meso* approach, the protein is delivered to the crystallization well dispersed in a lipidic mesophase. Optically, these can present

problems, especially at the mesophase/aqueous boundary, which invariably develops surface roughness. The rough surface scatters light and interferes with examination of the interior of the mesophase bolus, which is where the crystals usually form. The system is somewhat forgiving in the case of highly colored proteins such as bR. However, with small colorless crystals, surface roughness can mean that potential screen conditions are missed because the crystals go undetected. The problem can be overcome if the mesophase bolus is physically sandwiched between two optically clear surfaces. This eliminates the mesophase/aqueous medium interface and the corresponding roughness. The clear surfaces considered for the current application include glass and plastic plates. Plastic was eliminated because, without exception, all plastics have some degree of birefringence which compromises optical quality. Thus, glass was opted for and the plates so constructed were found to perform extremely well (see Fig. 2 in Cherezov & Caffrey, 2003). With glass there is no problem arising from birefringence and sub-microscopic crystallites can be seen when the wells are examined between crossed-polarizers (Fig. 2*g* in Cherezov & Caffrey, 2003). This is vital information that identifies conditions for subsequent optimization trials.

The glass plates that are used as a base for the crystallization wells have other features that make them particularly useful for robotic *in meso* crystallization. These include flatness (<±10 µm variation across the plate diagonal) and thickness (±50 µm variation in thickness between plates) uniformity. As will be pointed out below, the distance between the needle tip dispensing the cubic phase and the base of the crystallization well is critical for uniform and complete delivery of the cubic phase. Too large a distance and delivery does not occur. Too small a distance and delivery is incomplete. Thus, it is crucial that the correct distance be determined and that it is maintained while the plate is being loaded. Since the dispensing height of the syringe tip can be maintained within fairly tight limits by the robot itself, the flatness of the upper surface of the crystallization plate ultimately determines the effectiveness or otherwise of the delivery process. The plate sits on an aluminium block which in turn resides on the deck of the robot. The block has been machined and shimmed to produce a flat surface. Because the glass plates are uniformly flat and thick, when they are placed on top of the block successful and reproducible delivery in all 96 wells is essentially guaranteed. Thus, glass serves very well in this capacity. In addition, the adhesion between glass and the lipidic mesophase is quite strong, which facilitates delivery.

The crystallization plates were also designed with a view to making the imaging process as efficient as possible. With manual evaluation, the full volume of a sample is typically examined by continuously adjusting the depth of focus on the microscope. This can also be implemented with the automatic imager. However, it takes time. In the interests of eliminating the need to record images at different depths, the field depth of the imager optics was chosen to match the sample thickness. The latter was dictated by the thickness of the polyester spacer available commercially. Thus, with the instrument properly focused a single image is all that must be recorded to obtain an in-focus record of everything in the sample.

While the plates have many desirable properties, including the fact that the glass base and cover slip are reusable, they do suffer one major drawback. They are limited in that they can really only be used for screening purposes, where conditions are identified for crystal growth. The next step in the process is to harvest the crystal and to mount it in preparation for diffraction data collection. This is not particularly easy in these plates given that the upper and lower windows are made of glass, both of which become glued to the spacer. Since one of the plates is very thin cover glass and is extremely fragile, the likelihood of successfully separating the components cleanly is very low. It might be that a glass-cutter could be used for this purpose. One other possibility is to replace the upper cover slip with plastic. This could then be removed by cutting, with a scalpel for example, and the contents of the well exposed for crystal harvesting. The plastic would bring with it undesirable birefringence as already noted and would have to be suitably thick to provide hermetic well sealing. The approach taken in the laboratory currently is to use the plates for screening purposes only and to use Nunc 72-well microbatch plates (Hampton Research, Aliso Viejo, CA, USA) to grow crystals for harvesting. Leads found with the robot have been reproduced manually. Typically, when a successful condition is identified in an initial screen an optimization grid screening is performed with the robot. Optimized conditions are scaled up subsequently and performed manually in plates suitable for crystal harvesting. At this stage, a small adjustment in the
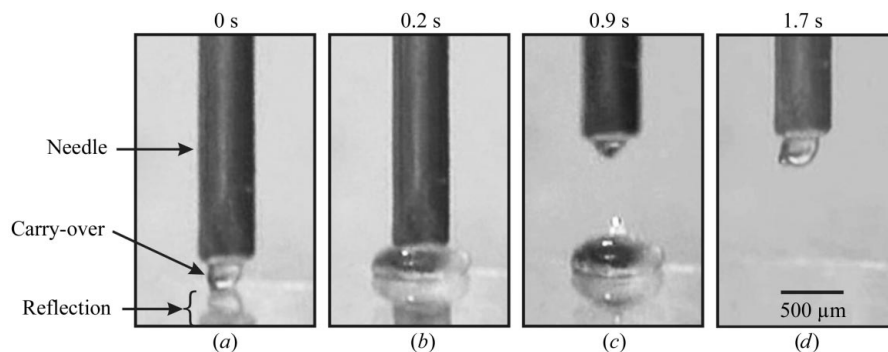

Figure 4
A time-lapse sequence of the lipidic cubic phase delivery process. 100 nl of the cubic phase is being delivered onto a glass surface. Elapsed time is indicated above each panel. (*a*) 'Carry-over' from the previous well is seen at the needle tip just before a fresh bolus is dispensed into the new well. (*b*) The bolus of cubic phase is being dispensed and is filling the space between the needle tip and the glass-plate surface. The distance between the needle tip and the plate surface is 250 µm. (*c*) Delivery is complete and the needle is being withdrawn from the plate. The dispensed cubic phase bolus takes on the shape of a flattened teardrop. Because the cubic phase is highly viscous and does not flow, the teardrop shape is stable in time. (*d*) The syringe and needle have moved on to the next well and what is referred to as 'carry-over' is seen developing at the needle tip. The latter is explained in more detail in the text. In (*a*)–(*c*) a reflection is seen on the glass surface.

concentration of the principal precipitant has been found to be useful.

After loading a plate, the final step involves capping with a glass cover slip. A brayer is used to produce a tightly sealed compartment within each well. However, since samples are stored for several weeks to months, water loss from the plate is a concern. While not quantified systematically for the current study, we have found that plates sealed in the usual way and stored at 293 K do not succumb to noticeable dehydration over a six-month period.

The base plate employed in the original version of the crystallization plate was used untreated and as supplied by the manufacturer. However, it was found that with some low surface tension precipitant solutions, particularly those containing alcohols, there was a tendency for the drop to spread on the plate and away from the bolus of cubic phase. To counteract this, the plates were silanized with Aqua Sil solution (Hampton Research, Aliso Viejo, CA, USA) following the manufacturer's recommendations. This corrected the problem. All of the base plates used for crystallization trials are now silanized. The adherence of the protein/lipidic mesophase to the glass surface does not appear to be compromised in any way by this treatment.

3.2. Crystallization robot

3.2.1. Dispensing the lipidic cubic phase. The robot described in this report is unique. What sets it apart from other robots is its focus on membrane-protein crystallization by the *in meso* method. This requires that the robot is capable of delivering accurately and reproducibly nanolitre volumes of a highly viscous lipid/protein dispersion. What makes this possible is the inclusion in the robotic device of a positive-displacement microsyringe with a motor-driven plunger and precise motorized positioning of the dispensing needle tip with respect to the well base. However, the robot would not be able
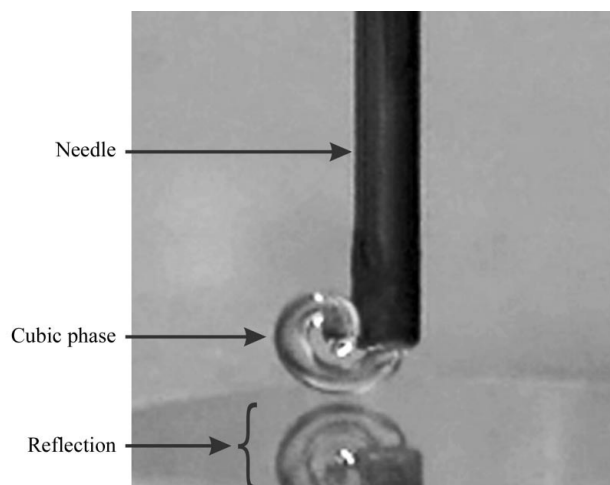
to function as such had we not been able to provision the dispensing syringe with relatively large volumes of homogenous lipid/protein dispersion. This was made possible by implementation of a mechanical mixing device developed in the laboratory for a related application (Cheng *et al.*, 1998). The robot introduced here achieves all of the above specifications and is now in routine use in the laboratory.

As might be expected, the performance of the robot is critically dependent on the reproducibility and accuracy with which it delivers the lipid/protein dispersion. Since the volumes and masses involved are very small and the speed at which things happen is high, it is not simple to quantify delivery with a view to identifying factors that impact on the quality of the delivery. To assist us in identifying such factors, we recorded the process using a video camera (Panasonic GP-KR222) and a $12\times$ zoom lens. Stills from the video recordings show the steps in the delivery process (Fig. 4). An examination of these data indicated that the following factors influence the
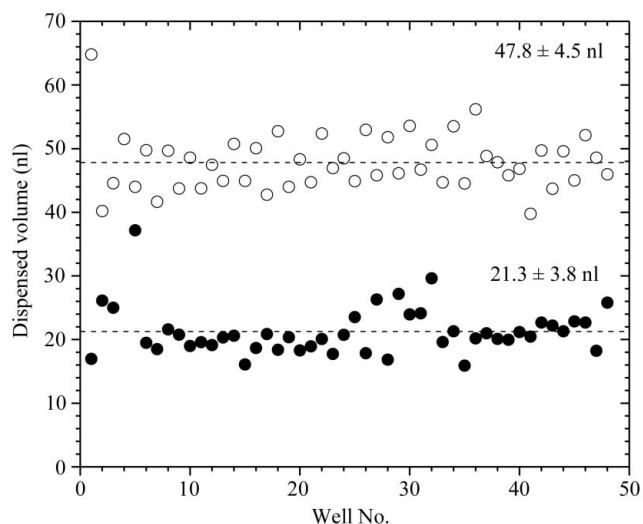
Figure 6
Precision and accuracy of the mesophase-dispensing component of the *in meso* robot. Repetitive measurements were performed using 20 nl (closed circles) and 50 nl dispensing volumes (open circles). Actual volumes dispensed were determined as described in §2. The average and standard deviation for each dispensed volume are indicated.
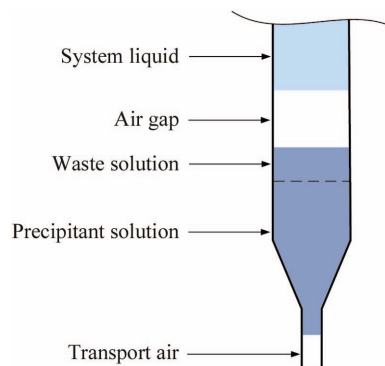
Figure 5
An example of an unsuccessful cubic phase bolus delivery. The failure arose because of the natural tendency of the dispensed tubular cubic phase to curl back on itself when the needle tip and the glass-plate surface are too far apart. In this case, 500 nl of cubic phase was dispensed at a tip-to-plate surface distance of 750 μm.

Figure 7
Schematic of a liquid (precipitant) handling tip in arm 1 of the *in meso* robot identifying the various adjustable parameters and components in the liquid-handling line. See text for details.

Table 1
Accuracy in dispensing of microlitre volumes of H_2O and 25%(w/w) PEG 4000 on a glass slide under optimized conditions.

The data represent statistics for at least 50 dispenses with each tip.

	H_2O (µl)	CV (%)	PEG 4000 (µl)	CV (%)
Tip1	0.98	7.2	0.93	7.9
Tip2	1.08	7.1	1.04	7.2
Tip3	0.95	11.3	0.96	11.1
Tip4	1.03	6.2	1.01	6.5

delivery process: dispersion composition and volume, needle tip-to-well base distance, needle-tip profile and diameter and the time profile of the delivery cycle. In our experience, the most important of these was the height of the dispensing needle tip above the well base. As shown in Fig. 5, when the height is too great the bolus of cubic phase emerges from the tip in the form of a tube which curls back on itself and away from the base of the well as it grows. In such an instance, there is no delivery. When the distance is too small, the bolus of cubic phase balls up around and sticks to the tip. Then when the syringe is withdrawn, so too is part or all of the dispensed bolus. Again, delivery fails. We have examined systematically the effect of tip-to-well distance on delivery and have established that for the bulk of the materials we have worked with so far a distance of between ~150 and 300 µm works well for dispensing volumes of 50 nl. We have not drawn up tables of optimum distances as a function of the assorted variables. These are all coupled to varying degrees and what we do in practice is to perform a quick test to establish the optimum distance for each new system we encounter. In addition to highlighting the importance of the dispensing height distance, this also serves to emphasize the need for accurate and precise z-positioning of the robot's arm 2 and for a flat receiving surface as provided by the glass base plate.

An examination of the video footage of the dispensing process revealed an interesting property of the viscous lipid/protein dispersion that impacts on effective delivery. This has to do with the fact that upon activating the syringe plunger to expel a set volume of the dispersion, the mesophase emerges from the needle tip at a rate that is slower than that expected from the plunger movement. Thus, there is a delay for complete elimination from the needle tip of the volume specified by moving the plunger. Depending on the system and the volumes involved, this can extend to several seconds. An indication of this is apparent when Figs. 4(c) and 4(d) are compared. We have not investigated the origin of the effect. It presumably has to do with the compressibility and the relaxation rate of the dispersion, which may include a small amount of trapped air. Initially, we considered the delay to be a problem. The sense was that we would need to wait at each well for complete expulsion of material before advancing to the next well. The time overhead of this would have made the delivery process unacceptably long (~20–25 min to complete a 96-well plate). However, we realised that provided the time for complete expulsion is less than the well-to-well duty cycle of the robot, then a steady state would be achieved. In this

case, each well will receive the allotted dispersion volume, with the exception of the first few wells, where pre-steady-state conditions prevail. Thus, in the interval when the needle tip is being moved out of one well (well A) and into position in another (well B), relaxation is taking place and material is exuding from the needle tip. Relaxation is complete by the time the tip is in place in well B. Accordingly, well B receives 'carry-over' from well A plus the amount dispelled in the time the tip is in place in well B. In essence, the volume that is lost to carry-over by a given well is made up by carry-over from the preceding well. To avoid pre-steady-state underfilling of wells for the first few dispenses, the syringe is 'primed' by expelling a small amount of the dispersion prior to loading the first well on the plate. We have evaluated the dispensing process for a standard volume of 50 nl cubic phase and the results are presented in Fig. 6. The data show that delivery has an associated standard deviation of within 10% of the target volume and that steady state is already established in the second well.

The smallest volume that can be dispensed using the current apparatus is 20 nl. However, the corresponding reproducibility is considerably less than with 50 nl with a standard deviation of 20% (Fig. 6). This is one of the reasons we have chosen to work with 50 nl as the standard volume with which to perform the bulk of our crystallization trials. Other reasons for working with the larger volume include the reduced effect of dehydration and the higher probability of crystallization (Cherezov & Caffrey, 2003).

3.2.2. Dispensing the precipitant solution. As noted, the robot has a liquid-handling arm (arm 1) and a lipidic mesophase-handling arm (arm 2). To ensure accurate dispensing of small volumes of precipitant solutions, each of the four liquid-handling tips on arm 1 was calibrated gravimetrically. Calibration was performed with 1 µl volumes since this is the precipitant volume currently in use for the bulk of the crystallization trials. Thus, 1 µl water was dispensed ten times into a small lightweight (500 mg) plastic tube and weighed using a microbalance (AX205, Mettler-Toledo Inc., Columbus, OH, USA). Weight was converted to volume using a density of 0.99823 g ml^{-1} (293 K, CRC Handbook of Chemistry and Physics). The procedure was repeated five times. Based on the average volumes delivered, a calibration factor was input into the program controlling the liquid handler to move each tip in the direction of the targeted volume. The procedure was repeated and for all four tips a dispensed volume within 5% of nominal was achieved.

With the dispensing-volume calibration completed, it was necessary to adjust the liquid-handling parameters for the different types of precipitant solutions to be used. This was performed with water and with a 25%(w/w) PEG 4000 solution to cover the range of viscosities likely to be encountered in a typical screening. The liquid-handling parameters included aspiration and dispensing speed and delays, air-gap volume, waste volume and transport air volume (Fig. 7). The values arrived at for the current configuration include aspiration and dispensing speeds of 50 µl s^{-1}, 0 s delays, 5 µl air-gap volume, 1 µl waste volume and 0 µl transport air volume. With these optimized parameters a coefficient of

variance (CV) of <8% was obtained for water and for a 25%(*w/w*) PEG 4000 solution (tip 3 has a slightly higher CV; Table 1).

3.2.3. Dehydration during setup. Under standard operation conditions, it takes about 13 min to fill (with 50 nl cubic phase and 1 µl precipitant solution) and to seal a 96-well plate. This means that the first well is exposed to the atmosphere for a period in which evaporation/condensation can occur and the contents of the precipitant solution can change. The length of exposure and attendant changes lessen with the well number on the plate. Naturally, the severity of the problem depends on the composition and volume of the precipitant solution and the relative humidity and temperature of the ambient environment. Our standard conditions include a 1 µl precipitant solution volume and room temperature (294–296 K). The relative humidity in the room where the screens are set up is not tightly regulated and varies from a low of ∼10% in the winter to a high of ∼70–80% in the summer. Since humidity is so variable, we quantified its effect on the changes undergone by 1 µl water in place of the precipitant during the course of a typical plate-loading process. The results (Fig. 8) show that evaporative loss is significant, amounting to 30% at 55% RH. We consider this level of loss to be unacceptable and set about reducing it by raising the RH of the environment in the immediate vicinity of the plate. This was performed using an ultrasonic humidifier (Sunbeam, model 626, Boca Raton, FL, USA), the output of which was directed in two streams in the general direction of the plate. With this new arrangement, providing ≥85% RH, the maximum loss was reduced to less than 10%, which was considered acceptable. Local humidification of the type described is now a part of our standard crystallization screen set-up.

3.3. Imaging station

3.3.1. Performance characteristics. The primary purpose of the image station is to record a high-quality image of the contents of the crystallization well. The emphasis is on image quality, as it is this that determines what will and will not be seen in the visual inspection of the image. It ultimately defines the success of the overall screening process. We already had in place a standard set of conditions for crystallization and a plate in which to perform the trials. The plates have unequalled optical properties since the critical elements are made of glass. The specifications on the imaging system were therefore to provide the highest quality image without the need for sampling along the optical axis of the sample and to image a large enough area of the well to include the bolus of cubic phase. The latter should accommodate a bolus 700 µm in diameter and for positional variability of the bolus in the imaging (*x, y*) plane as dictated by arm 2 of the robot.

One of the critical elements of any imaging device is the lens. Both the resolution R and the depth of field DF depend on the numerical aperture NA of the lens in the following way: $R = 0.61\lambda/\mathrm{NA}$, $\mathrm{DF} = n\lambda/NA^2$, where λ is the wavelength of light ($\lambda \simeq 500$ nm) and n is the refractive index ($n = 1$ for air).

NA is defined as the sine of the angle between the marginal ray and the optical axis of the lens multiplied by n.

After testing several lenses we settled on the Navitar 12× zoom lens as a good compromise between lens characteristics, image quality and price. Continuous zoom provides the ability to adjust magnification, which of course is tied to field of view and numerical aperture. Our standard imaging protocol is to scan each plate with a 3× zoom. At this magnification, NA = 0.051, DF $\simeq$ 190 µm and $R \simeq 6.0$ µm. Thus, the entire contents of the well, which is 130 µm thick, is in focus with a resolution that is good enough to see micrometre-sized crystals in a bolus that is ∼700 µm in diameter. The field of view of the half-inch CCD sensor in the Qimaging Micropublisher camera that is used in recording is 2.4 × 1.8 mm, which allows for some variability in bolus positioning in the imaging plane. This represents an image with 2048 × 1532 pixels.

The imaging system is required to image all wells in a crystallization plate. This is performed either by moving the imager or by moving the plate. We have chosen the latter option using a high-precision *xy*-translation stage upon which to mount the plate. The stage has a positional accuracy of 6 µm, which is considerably better than the accuracy of arm 2 of the robot (200 µm). Accordingly, it is the latter that limits the overall performance of the imager. As noted, the area imaged has been increased to compensate for this positional variability in sample positioning.

Speed is of the essence in any high-throughput robotic system. Thus, the rate at which the imaging can be executed is critical to overall throughput. This has two principal components: the rate at which the translation stage moves from well to well and the time to transfer the image into storage. With
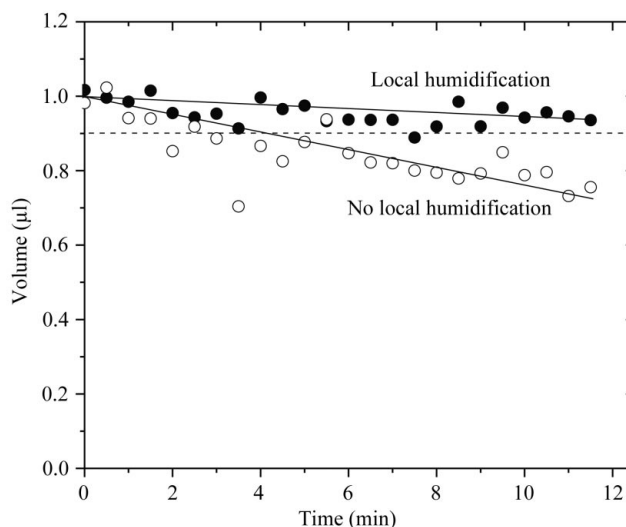

Figure 8
Dehydration of 1 µl water drops during the course of a typical 96-well filling operation by the *in meso* robot. Throughout the filling process, the wells were uncovered and exposed to the atmosphere. Filling was carried out at 293 K with (>85% RH; solid circles) and without local humidification (∼55% RH; open circles). The time to complete the filling operation was ∼13 min. Data points at long and short times correspond to wells on the 96-well plate that were filled first and last, respectively. Drop volume was determined as described in §2.
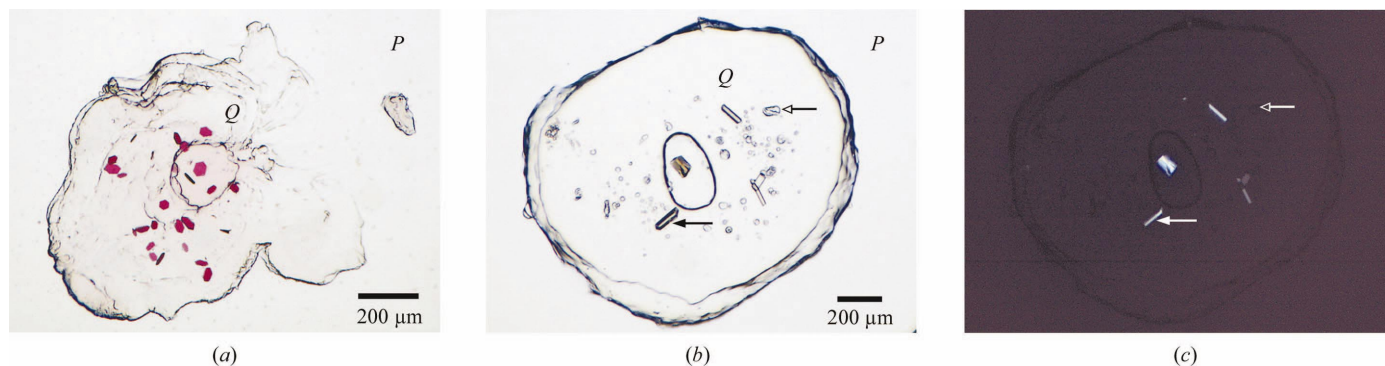
Figure 9
Digital photographs of (*a*) membrane protein (bacteriorhodopsin) and (*b*) and (*c*) water-soluble protein (lysozyme) crystals grown using the *in meso* robot and recorded using the imaging robot. All crystallizations were performed in the monoolein cubic mesophase at 293 K. The bolus of mesophase [50 nl in (*a*) and 200 nl in (*b*), labeled *Q*] is in the center of the image and is surrounded by precipitant solution (labeled *P*). The protein crystals in (*a*) are reddish purple in color, while those in (*b*) and (*c*) are colorless. Images (*a*) and (*b*) were recorded with polarized light. The image in (*c*) is the same as in (*b*) except that it was recorded between crossed polarizers. The open headed arrows in (*b*) and (*c*) point to a non-birefringent bubble. The solid-headed arrows in (*b*) and (*c*) point to a birefringent crystal. Parenthetically, we note that (*a*) does not faithfully represent the shape of the mesophase that was used for image analysis and for delivered volume quantitation described in §3.2.1 and in Fig. 6. In (*a*) there was a phase change upon the addition of precipitant which caused the shape of the lipidic bolus to change and to become irregular.
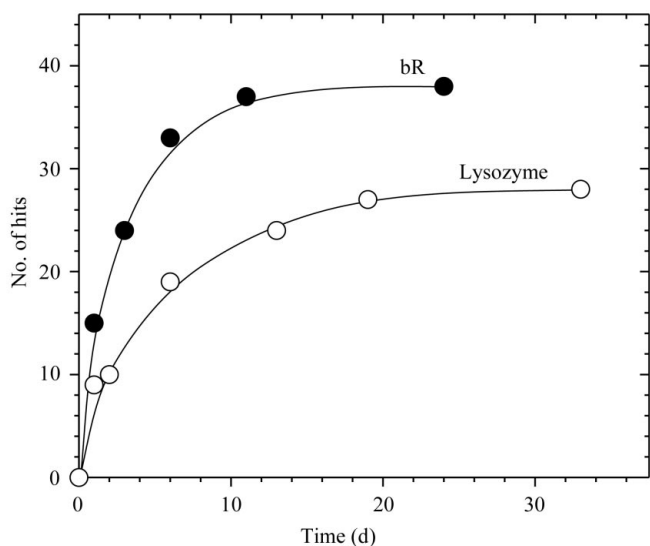

Figure 10
Progress in the crystallization of bacteriorhodopsin and of lysozyme in the monoolein cubic phase using the *in meso* robot. Trials were set up as described in the text (§3.4.1). For both proteins, a total of 480 conditions were screened in duplicate. A hit was registered when an identifiable crystal (usually ≥ 5 μm in maximum dimension) was observed in the well. In the case of bacteriorhodopsin, submicrometre-sized 'crystals' that appeared as bluish dots of birefringence were also included in the list of hits. These were particularly prevalent under conditions close to those that yield readily identifiable crystals.

the current arrangement, a 96-well plate can be scanned and images stored in 4.5 min.

3.3.2. Image processing. Digital images of individual wells on each crystallization plate are recorded using a CCD camera in a 16-bit unprocessed format. In the interests of time, each raw 2048 × 1532 pixel image is stored on a computer directly and processing is performed later, consisting of Bayer interpolation, white-balance adjustment and image enhancement. The latter is implemented using *Adobe Photoshop Actions* in batch mode and involves corrections of 'white' and 'black' points, shadow recovery, increasing contrast and image down-

sampling (to 1024 × 768 pixels) and sharpening. Special *Photoshop Actions* have been optimized to process the following image types: colored protein images, colorless protein images and images recorded between crossed polarizers.

With these image-processing features in place, crystals larger than 10 μm are usually easily recognized. A selection of processed images is shown in Fig. 9.

Formation of droplets and other inhomogeneities in the lipidic mesophase are not infrequent events. They can significantly obstruct the view and can give rise to false positives where crystals are identified incorrectly (Fig. 9*b*). However, the ambiguity can be resolved in the case of birefringent crystals by examining the corresponding image recorded between crossed polarizers (compare Figs. 9*b* and 9*c*).

3.4. Crystallization trials

3.4.1. In meso. By way of demonstrating the performance of the new *in meso* robot, crystallization trials have been performed with our benchmark membrane protein, bacteriorhodopsin (bR), and with the water-soluble lysozyme. For the former, 50 nl bR-laden cubic phase and 1 μl of precipitant solution was used. With the latter, trials consisted of 200 nl lysozyme/monoolein mix and 0.5 μl precipitant solution. Trials included the following commercially available screens: Crystal Screen HT, Index HT, Wizard I and II, SaltRx and JBScreen, representing a total of 480 conditions, and were performed in duplicate for both proteins.

Both crystallization experiments were monitored for at least a month. Crystallization trials produced 38 hits (7.9% success rate) in the case of bR and 28 hits (5.8% success rate) in the case of lysozyme (see supplementary material for a complete list of successful conditions[1]). The most successful

---

[1] Supplementary material has been deposited in the IUCr electronic archive (Reference: TM5010). Details for accessing these data are described at the back of the journal.
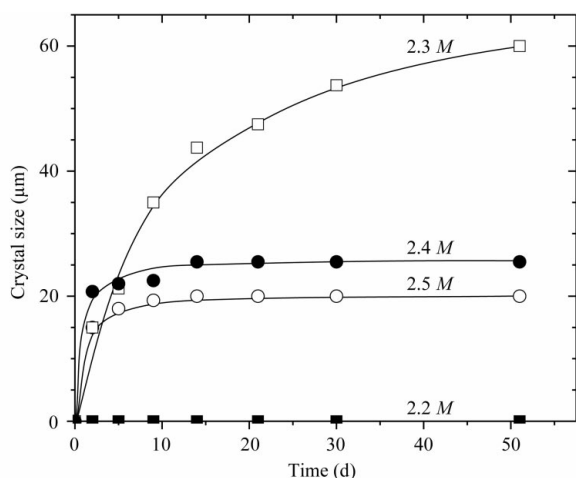
Figure 11
Kinetics of bacteriorhodopsin crystal growth in 96-well glass plates set up using the *in meso* robot and its dependence on sodium potassium phosphate pH 5.6 concentration at 293 K. The concentration of precipitant is indicated. Four replicates were used for each time point. Crystal size refers to the maximum dimension of the crystals (usually hexagonal plates, see Figs. 12*a* and 9*a*) in a given well. The reported value is the average over all replicates at a given time. Trials were performed using 60%(*w*/*w*) monoolein and 40%(*w*/*w*) protein solution (15.9 mg ml^{-1} protein). Cubic phase and precipitant volumes were 50 nl and 1 µl, respectively.
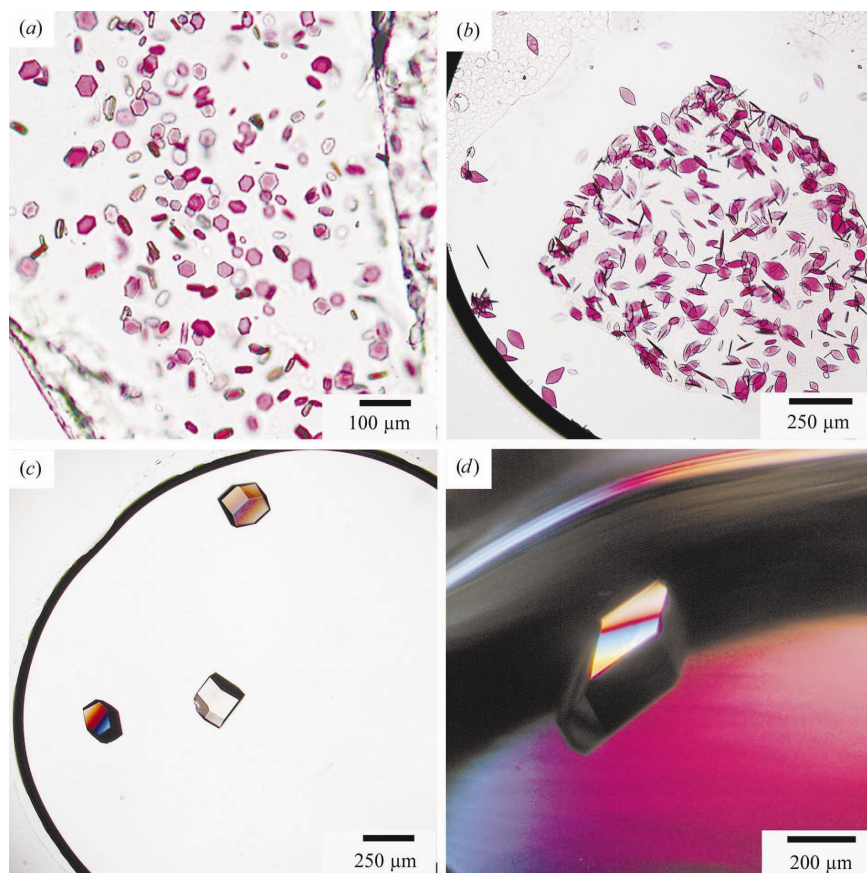

Figure 12
Protein crystals grown by different crystallization methods using the *in meso* robot. (*a*) Crystals of bacteriorhodopsin grown by the *in meso* method after 5 d at 293 K. (*b*) Crystals of bacteriorhodopsin grown by the bicelle method after 7 d at 310 K. (*c*) Crystals of lysozyme grown by the microbatch method after 1 d at 293 K. (*d*) Crystals of lysozyme grown by the sitting-drop vapor-diffusion method after 5 d at 293 K.

crystallants for bR include ammonium citrate, ammonium phosphate, ammonium sulfate, lithium sulfate, sodium nitrate and sodium/potassium phosphate. Lysozyme crystallants included ammonium chloride, ammonium nitrate, sodium chloride, sodium nitrate, sodium formate, sodium malonate, PEG 3350 and PEG 8000. Fig. 10 shows the progression in the number of hits observed in the crystallization trials of the two proteins. It is interesting to note that 1 d post-setup approximately one third of the total number of hits have already been identified and that no new hits appear after ∼18 and ∼28 d in the case of bR and lysozyme, respectively.

The dependence of the growth characteristics of bR crystals *in meso* on crystallant concentration is described in Fig. 11. The metric for growth was the maximum dimension of the hexagonal plate-like crystals that typically form in the case of bR. Because the plates are usually thin, a measurement of plate thickness is often quite difficult to make. Thus, 2.2 *M* sodium/potassium phosphate (SPP) did not support crystal growth for the duration of the study (50 d). However, at 2.3 *M* SPP growth was rapid and sustained. In fact, crystals at 60 µm were continuing to grow at the last time point in the study. Increasing the crystallant concentration to 2.4 and 2.5 *M* had a dramatic effect on growth in that the maximum dimension of about 20 µm was achieved within a week. These data suggest that optimization within the 2.2–2.4 *M* SPP concentration range is likely to yield even larger more slowly growing crystals. Parenthetically, we have observed that the ratio of plate thickness to its maximum dimension usually increases with SPP concentration and that when crystals stop growing in-plane they can continue to grow in thickness.

3.4.2. Microbatch. To demonstrate the versatility of the *in meso* robot it was configured to set up crystallization trials by the microbatch method. The results are presented in Fig. 12(*c*), in which large crystals of lysozyme grown in this way are clearly visible.

3.4.3. Sitting-drop vapor diffusion. The *in meso* robot can also be used to perform vapor-diffusion-based crystallization. In this case, sitting drops containing lysozyme were set up that went on to produce large crystals (Fig. 12*d*).

3.4.4. Bicelle method. bR crystallization by the bicelle method was carried out successfully using the new *in meso* robot. The results are shown in Fig. 12(*b*). As noted in §2.5.4, trials were performed as a function of precipitant concentration and dehydration across the 96-well plate. Best crystals were obtained in wells *B*9, *C*9 and *D*9 corresponding to 3.2–3.6 *M* sodium dihydrogen phosphate and a

relatively short period (< 4 min) of exposure for evaporative loss.

3.5. Improvements

The instrumentation just described is now in routine use in our laboratory. However, there are elements of both the robot and the imaging station that could benefit from improvement. In the first instance, it is desirable to speed up the crystallization plate-loading process so that samples have less time to succumb to evaporative loss. As noted, the current filling time is about 13 min. We expect to be able to cut this time in half by writing and implementing more efficient robot-controlling programs and by effecting simultaneous arm motion.

It is imperative that finding the x, y and z coordinates of well 1 of a given plate is performed with great care and accuracy because the accuracy with which the rest of the plate is filled depends on it. Currently, this is performed manually and takes some time. We would like to automate the process and we have proposed the use of what is called a 'soft-sensor' for coordinate measurement (Muthusubramaniam *et al.*, 2004). Briefly, this involves using a small bolus of cubic phase at the dispensing-needle tip to register when the tip is close to contacting the base of the well. This is a work in progress and has not been settled on as the route to follow, and other options are being examined.

As noted, the relative humidity of the environment in which screens are set up has a profound effect on the final composition of the screen. Currently, we very roughly control the local environment of the plate in a way that reduces evaporative loss to an acceptable level. We can and will do better by enclosing the robot in a windowed chamber where RH will be regulated in the 85–90% range under computer control.

The current plate/robot configuration produces a disc-shaped bolus of mesophase. The rate at which equilibration with the crystallant solution ingredients occurs and the exact time profile of these events during the course of the crystallization trial depends on location within the bolus. A greater range of conditions within a given well would be realised were it possible to tailor-make the bolus shape. Given the current set-up, this is limited to discs, elongated slabs and wedges. While we have not experimented with shape as a variable with regard to crystallization behavior, we have been able to produce boluses having an assortment of shapes. This is one area worthy of investigation that might improve the overall crystallization success rate.

Crystals, once they form, must be harvested and mounted for diffraction measurements. These are slow steps that are currently performed manually. We are exploring ways of automating both processes and some preliminary results have been reported (Chen *et al.*, 2004). To effect automatic harvesting with the *in meso* system, however, will require that we also overcome the difficulty of crystal recovery from within the glass-windowed wells currently in use.

Once filled and capped, plates are placed in temperature-controlled incubators. They are then evaluated manually and at the image station on a defined schedule. Moving toward higher throughput will necessitate reliance on the image station completely and on automatic transfer of plates between the incubator and imaging station. An industrial-grade robot is being considered for the latter application.

The manual scoring of crystallization trials is a definite bottleneck in the current setup. We are working on automatic image-recognition and scoring programs optimized to evaluate images of *in meso* crystallization trials taken with the imaging station. This task is much more challenging than evaluation of crystallization trials of soluble proteins set up using conventional methods since the lipidic mesophase often develops imperfections and/or droplets that have sharp edges and facets. Images taken using cross-polarizers will be used to aid in crystal identification in those cases.

Bar-coding for plate identification and tracking has not yet been implemented but will be shortly. Bar-coded labels will be attached to the plates (Fig. 1*a*) and will be identified and logged by means of a reader fitted to the image station. It will be imperative to have the bar-coding system in place when a robotic plate manipulator to move plates between the incubator and the image station is installed.

Finally, to handle and to mine efficiently the wealth of data associated with a crystallization project such as this, a comprehensive database framework is needed. Accordingly, we are in the process of designing and implementing a relational database for archiving crystallization trial-related data. This includes everything from an inventory of lipids, proteins and crystallants used in trials all the way to scores of the trials themselves. We would also like to implement a web-based data-mining interface to the above database to support more rationally designed crystallization trials based on an analysis that includes conditions producing hits as well as misses.

4. Conclusions

A robot for setting up crystallization trials with an emphasis on membrane proteins has been developed. The robot was assembled from commercially available components and is relatively inexpensive. It was designed to perform crystallizations of membrane proteins from within the highly viscous lipidic cubic mesophase and it does so in a way that is extremely economical in terms of protein, lipid and precipitant. Standard crystallization conditions call for just 20 nl protein solution, 30 nl lipid and 1 µl precipitant solution. Where necessary, it is possible to reduce these volumes by a factor of 2.5. Under standard conditions, precipitant and mesophase volume delivery is reproducible.

The crystallization robot is quite versatile in that it can be used not only for *in meso* trials but also for vapor-diffusion, microbatch and bicelle crystallizations. In this study, we have shown that the robot works equally well with membrane and soluble proteins.

96-well glass-based crystallization plates have been designed and built for use with the *in meso* robot. They have exquisite optical properties that lend themselves to visualizing microcrystals and to birefringence-free examination between

crossed polarizers. The plates have a very small profile height, facilitating high-density storage. The plate footprint and 96-well layout follow SBS standards. The polyester tape used to create the wells is relatively water-tight. Thus, dehydration of well contents is not a problem when storage is carried out under moderate conditions. Well contents are sandwiched between two glass plates and are mechanically quite stable such that the plates do not require careful handling. The glass plates are themselves reusable.

To cope with the high throughput of trials made possible by the crystallization robot, an automated imaging system has been designed and built, once again using commercially available components. Its optics are matched to the well thickness of the glass crystallization plates such that the complete volume of the mesophase bolus can be imaged in a single shot. A 96-well plate can be imaged in 4.5 min. The slower image processing is performed subsequently off-line.

The robots introduced here will enable high-throughput crystallization trials of membrane proteins using lipidic mesophases with unprecedented speed and with microgram quantities of protein. This means that more membrane protein targets will be subjected to crystallization trials by way of the *in meso* method with relatively fast turnaround. As more targets are examined, the utility of the *in meso* method for membrane-protein crystallization will be more completely evaluated. This automation will contribute in no small measure to accelerating the pace of research into and our understanding of the relationship between the structure and function of membrane proteins.

References

Caffrey, M. (2003). *J. Struct. Biol.* **142**, 108–132.

Chen, W., Peddi, A., Zheng, Y. F. & Caffrey, M. (2004). *Proceedings of the World Congress on Intelligent Control and Automation, Hang Zhou, People's Republic of China.*

Cheng, A. H., Hummel, B., Qiu, H. & Caffrey, M. (1998). *Chem. Phys. Lip.* **95**, 11–21.

Cherezov, V. & Caffrey, M. (2003). *J. Appl. Cryst.* **36**, 1372–1377.

Dencher, N. A. & Heyn, M. P. (1982). *Methods Enzymol.* **88**, 5–10.

Faham, S. & Bowie, J. U. (2002). *J. Mol. Biol.* **316**, 1–6.

Lanyi, J. K. & Schobert, B. (2002). *J. Mol. Biol.* **321**, 727–737.

Misquitta, Y. & Caffrey, M. (2003). *Biophys. J.* **85**, 3084–3096.

Muthusubramaniam, L., Peddi, A., Zheng, Y. F., Cherezov, V. & Caffrey, M. (2004). *Proceedings of the IEEE International Conference on Robotics and Automation*, pp. 1450–1455. Piscataway, NJ, USA: IEEE.

Nollert, P., Qiu, H., Caffrey, M., Rosenbusch, J. P. & Landau, E. M. (2001). *FEBS Lett.* **504**, 179–186.

Schobert, B., Cupp-Vickery, J., Hornak, V., Smith, S. O. & Lanyi, J. K. (2002). *J. Mol. Biol.* **321**, 715–726.